ÉCOLE POLYTECHNIQUE FÉDÉRALE DE LAUSANNE
MATHICSE
Mathematics Institute of Computational Science and Engineering
School of Basic Sciences - Section of Mathematics

MATHICSE Technical Report
Nr. 3.2012
February 2012

Boundary control and shape optimization for the robust design of bypass anastomoses under uncertainty

Toni Lassila, Andrea Manzoni, Alfio Quarteroni and Gianluigi Rozza

http://mathicse.epfl.ch

Phone: +41 21 69 37648

Address:
EPFL - SB - MATHICSE (Bâtiment MA)
Station 8 - CH-1015 - Lausanne - Switzerland

Fax: +41 21 69 32545

Boundary control and shape optimization for the robust design of bypass anastomoses under uncertainty

Toni Lassila[♯], Andrea Manzoni[♯], Alfio Quarteroni[♯,†], Gianluigi Rozza[♯*]

February 2, 2012

[♯] CMCS - Modelling and Scientific Computing,
MATHICSE - Mathematics Institute of Computational Science and Engineering,
EPFL - Ecole Polytechnique Fédérale de Lausanne,
Station 8, CH-1015 Lausanne, Switzerland.

[†] MOX– Modellistica e Calcolo Scientifico,
Dipartimento di Matematica "F. Brioschi",
Politecnico di Milano,
P.za Leonardo da Vinci 32, I-20133 Milano, Italy.

Abstract

We review the optimal design of an arterial bypass graft following either a *(i)* boundary optimal control approach, or a *(ii)* shape optimization formulation. The main focus is quantifying and treating the uncertainty in the residual flow when the hosting artery is not completely occluded, for which the worst-case in terms of recirculation effects is inferred to correspond to a strong orifice flow through near-complete occlusion. Worst-case optimization is performed to identify an anastomosis angle and a cuffed shape that are robust with respect to a possible range of residual flows. We also consider a reduced order modelling framework based on reduced basis methods in order to make the robust design problem computationally feasible.

Keywords: optimal control, shape optimization, arterial bypass grafts, uncertainty, worst-case design, reduced order modelling, Navier-Stokes equations.

Introduction

Atherosclerosis is a pathology of the arterial system which is driven by the accumulation of fatty materials such as cholesterol in the lumen. As a result the arterial wall first thickens as the plaque grows and in a subsequent stage narrows, leading to partial or total occlusion. Bypass grafts can provide blood flow

*Corresponding Author, E-mail: `gianluigi.rozza@epfl.ch`

through an alternative bridging path in order to overcome critically occluded arteries. One of the most dangerous cases is related to coronary arteries, which supply the oxygen-rich blood perfusion to the heart muscle. The lack of an adequate blood supply may cause tissue ischemia and myocardial infarctions. Coronary Artery Bypass grafting is a standard surgical procedure to restore blood perfusion to the cardiac muscle by redirecting blood from the Aorta through a graft vessel (either artificial or biological) to the downstream of the occluded coronary artery. The design of the end-to-side anastomosis that connects the graft vessel to the host vessel is a critical factor in avoiding post-operative recurrence of the stenosis, since fluid dynamic phenomena such as recirculation, oscillating or untypically high/low shear rates, and stagnation areas can cause the growth of another stenosis downstream from the anastomosis. Different kinds and shapes for aorto-coronaric bypass anastomoses are available, such as Miller cuffed models or Taylor patches [28, 17]. The connection of the graft to the coronary artery can be done using an end-to-side or a side-to-side anastomosis; a detailed survey of the predominant flow features of end-to-side anastomoses is provided in [28]. The major factors known to strongly influence the recurrence of intimal hyperplasia are related to Wall Shear Stress (WSS) and vorticity in the region close to the anastomosis. Hence, a typical attempt to design a bypass graft is apt at minimizing some cost functionals related to these physical indices of interest.

Numerical methods of Computational Fluid Dynamics (CFD) can help in understanding local haemodynamics phenomena and the effect of vascular wall modification on flow patterns (see e.g. [28]). On the other hand, theoretical methods of optimal control and shape optimization enable a suitable formulation of the optimal design problem for bypass grafts. Many works [2, 1, 25, 30, 33, 34, 38, 40] have focused in the last decade on the optimal shape design of end-to-side anastomoses, typically by acting on the wall shape near the anastomosis by local shape variations. The three most significant design variables in end-to-side anastomoses are [28]: the anastomosis angle, the graft-to-host diameter ratio [23], and the toe shape (see Fig. 1). Also the flow split between the proximal outflow segment and the distal outflow segment affects greatly the distribution of WSS [13], as do the viscosity and the Reynolds number. The effect of the flow profile at or near the inlets must also be taken into account. The near-complete occlusion of stenotic arteries produces the largest (often turbulent) disturbances in the flow, and has been linked to triggering biochemical processes such as thrombosis, hemolysis etc. While it is known that the physical unsteady and pulsatile flow can be replaced with a steady mean flow with the same Reynolds number for purposes of evaluating the mean WSS distribution [12, 11], the correct flow profile must be taken into account if accurate WSS predictions are desired[a]. In conclusion, it seems clear that in order to design a

[a]For example, in [43] the effect of cardiac motion on the flow in a coronary artery was studied: it was shown that the motion-induced change in the velocity profile could impact the

bypass graft in a robust way, one must be prepared to take into account all the various sources of *uncertainty* that can effect the final optimized design.

Only recently the effect of uncertainty in the design of bypass grafts has been taken into account. In [40] the bypass configuration was optimized under unsteady flow with an uncertain flow split between the occluded artery and the graft. The robust design was sought by minimizing a cost functional that measured the area of low wall shear stress in the downstream region of the anastomosis. To make the design robust, the authors added a penalty term for the standard deviation of the output due to input uncertainties. The cost of such an optimization method was reported as quite high, 11 days in the fully 3D unsteady case on a 18×4 cores parallel cluster. In [25] a similar problem was considered for steady 2D flow, but optimizing the whole shape rather than just the angle. The computational cost was diminished by introducing a Reduced Order Model (ROM) for the fluid equation based on Reduced Basis (RB) methods, making the robust design problem computationally feasible. In [33] the bypass shape was obtained by minimizing the total shear rate, and the sensitivity of the optimal shape with respect to the uncertain viscosity in a non-Newtonian rheology was considered. There was no attempt made to find a robust optimal shape over a range of viscosity values, likely due to prohibitive cost of running the full-fidelity three-dimensional finite element simulations.

These preliminary works already indicate that in presence of uncertainty effects the bypass design problem is not yet satisfactorily solved by existing classical computational approaches, and, furthermore, that some type of ROM is needed to reduce the computational cost. In particular, a new contribution of this work is aimed at inserting some uncertainty elements (featuring the nature of the residual flow in the partially occluded arterial branch) in both an optimal control and a shape optimization problem, solved within a suitable reduced framework, in view of simultaneous computational and geometrical reduction. We also test whether our simplifications affect the robust design obtained with or without the reduction to a pure boundary control problem, as well as comparing results between 2D and 3D.

In this work we review some features related to the optimal design of bypass grafts (Sect. 1) and present two different paradigms based on optimal control and shape optimization, highlighting key points and difficulties. In the first case, a simplified 2D boundary control formulation is considered (Sect. 2), incorporating uncertainty about residual flows through the stenosed artery. In the second case, a 2D shape optimization problem is considered (Sect. 3), dealing with robust design under uncertainty. For the sake of computational saving, these problems are solved within a suitable ROM framework, presented in Sect. 4. Numerical results, as well as a comparison with simplified 3D configurations, are detailed in Sect. 5-6, followed by some conclusions in Sect. 7.

WSS values by up to 150%.

1 Mathematical modelling for bypass optimal design

Haemodynamic factors like flow recirculation or stagnation, as well as high vorticity or dissipation regions, low and oscillatory WSS, play a driving role in the development of vascular diseases. Hence, meaningful mathematical models and description of blood flows, together with accurate numerical simulations, can have useful clinical applications especially in surgical procedures. However, a rigorous model for blood circulation should take into account *(i)* the flow unsteadiness, *(ii)* the arterial wall deformability, described by suitable structural models [21] and possibly *(iii)* complex rheological model to characterize the aggregate nature of the blood [37]. In view of studying optimal control and shape optimization problems, which entail the repeated simulation of these flow equations (and the evaluation of the cost functional to be minimized), we cannot afford the solution of PDE models involving such complex features – computational costs would be too prohibitive. For these reasons, we model blood flows adopting steady incompressible Navier-Stokes equations for laminar Newtonian flow with the velocity field $\mathbf{v}$ and pressure field p satisfying

$$\begin{cases} -\nu\Delta\mathbf{v} + (\mathbf{v}\cdot\nabla)\mathbf{v} + \nabla\mathbf{p} = \mathbf{f} & \text{in } \Omega \\ \nabla\cdot\mathbf{v} = \mathbf{0} & \text{in } \Omega \\ \mathbf{v} = \mathbf{u_{bc}} & \text{on } \Gamma_{bc} \\ \mathbf{v} = \mathbf{u_{in}} & \text{on } \Gamma_{in} \\ \mathbf{v} = \mathbf{0} & \text{on } \Gamma_{w} \\ -p\mathbf{n} + \nu\dfrac{\partial\mathbf{v}}{\partial\mathbf{n}} = \mathbf{0} & \text{on } \Gamma_{out}. \end{cases} \tag{1}$$

Here $\Omega \subset \mathbb{R}^d$ for $d = 2, 3$ is assumed to be piecewise C^2 with convex corners, representing an end-to-side anastomosis (see Fig. 1). The Dirichlet portion Γ_D of the boundary is further divided into the inlet from the stenosed section of the artery Γ_{in} and the bypass inlet Γ_{bc}, where we prescribe two inflow profiles $\mathbf{u}_{\mathrm{in}}$ and $\mathbf{u}_{\mathrm{bc}}$ respectively, and the walls, where we prescribe a no-slip boundary condition. We assume a free-stress boundary condition at the outlet $\Gamma_{\mathrm{out}} \neq \emptyset$. Moreover, blood dynamic viscosity is $\mu = 0.04\ \mathrm{g\,cm^{-1}\,s^{-1}}$, blood density $\rho = 1\ \mathrm{g\,cm^{-3}}$, thus yielding a kinematic viscosity $\nu = \mu/\rho = 0.04\ \mathrm{cm^2\,s^{-1}}$ and a Reynolds number $Re = \tilde{v}D/\nu$ of order 100. The corresponding weak form of Navier-Stokes equations (1) reads: find $(\mathbf{v}, p, \boldsymbol{\eta}) \in \mathcal{Y}\times\mathcal{Q}\times\mathcal{G}$ s.t.

$$\begin{aligned} \mathcal{A}(\mathbf{v}, p, \boldsymbol{\eta}; \mathbf{z}, q, \boldsymbol{\lambda}) :=& a(\mathbf{v}, \mathbf{z}) + b(p, \mathbf{z}) \\ &+ b(q, \mathbf{y}) + c(\mathbf{v}, \mathbf{v}, \mathbf{z}) + g_D(\boldsymbol{\eta}, \mathbf{z}) + g_D(\mathbf{u} - \mathbf{u_D}, \boldsymbol{\lambda}) = 0, \end{aligned} \tag{2}$$

for all $(\mathbf{z}, q, \boldsymbol{\lambda}) \in \mathcal{Y}\times\mathcal{Q}\times\mathcal{G}$, where the continuous bilinear and trilinear forms are defined as

$$a(\mathbf{v}, \mathbf{z}) := \nu\int_\Omega \nabla\mathbf{u} : \nabla z\, d\Omega, \quad b(p, \mathbf{z}) := \int_\Omega p \ \mathrm{div}\ z\, d\Omega,$$

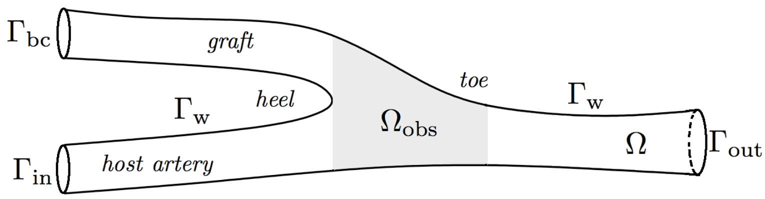

Figure 1: A schematic view of a bypass graft anastomosis.

$$c(\mathbf{v},\mathbf{w},\mathbf{z}) := \int_\Omega (\mathbf{v}\cdot\nabla)\mathbf{w}\cdot\mathbf{z}\,d\Omega,$$

and the bilinear form

$$g_D(\mathbf{v},\mathbf{w}) := \int_{\Gamma_D} \mathbf{v}\cdot\mathbf{w}\,d\Gamma$$

is used to enforce a Dirichlet boundary condition on $\Gamma_{\rm in}\cup\Gamma_{\rm w}\cup\Gamma_{\rm bc} =: \Gamma_D \subset \partial\Omega$ with boundary data $\mathbf{u}_D$. The velocity space is chosen as $\mathcal{Y} := [H^1(\Omega)]^d$, the pressure space as $\mathcal{Q} := L^2(\Omega)$, and the Lagrange multiplier space $\mathcal{G} := [H^{-1/2}(\Gamma_D)]^d$. We denote $\mathbf{L}_{\rm bc}, \mathbf{L}_{\rm in} \in \mathcal{Y}$ two divergence-free lifting functions of the boundary data $\mathbf{u}_{\rm bc}$ and $\mathbf{u}_{\rm in}$, such that $\mathbf{L}_{\rm bc}|_{\Gamma_{\rm bc}} = \mathbf{u}_{\rm bc}$ and $\mathbf{L}_{\rm in}|_{\Gamma_{\rm in}} = \mathbf{u}_{\rm in}$ on $\Gamma_{\rm bc}$ and $\Gamma_{\rm in}$, respectively. Moreover, in order to have a physically meaningful problem, we enforce the total conservation of fluxes between the (partially or totally) occluded branch Γ_{in} and the graft inlet Γ_{bc}, according to

$$Q_{\rm in}+Q_{\rm bc} = \int_{\Gamma_{\rm in}} \mathbf{v}_{\rm in}\cdot\mathbf{n}d\Gamma + \int_{\Gamma_{\rm bc}} \mathbf{v}_{\rm bc}\cdot\mathbf{n}d\Gamma = \int_{\Gamma_{\rm in}} \mathbf{v}_{\rm in}\cdot\mathbf{n}d\Gamma =: Q_{\rm tot}\ \text{(constant)}. \quad (3)$$

To show the well-posedness of the inhomogeneous Navier-Stokes equations (2), we cite a classical stability and uniqueness result under the assumption of *small data* (for the proof, see e.g. [41], Chapter 2, Theorem 1.6):

Lemma 1. *Assume that* $\mathbf{u}_{in} \in [H^{1/2}(\Gamma_{in})]^d$, $\mathbf{u}_{bc} \in [H^{1/2}(\Gamma_{bc})]^d$ *and* Ω *is of class* C^2. *The velocity field* $\mathbf{v} \in \mathcal{Y}$ *defined as the solution of (2) satisfies the stability estimate*

$$\|\mathbf{v}\|_1 \leq \frac{2}{\nu}\|\widetilde{f}(\mathbf{L}_{in},\mathbf{L}_{bc})\|_{-1},$$

where

$$\|\widetilde{f}(\mathbf{L}_{in},\mathbf{L}_{bc})\|_{-1}^2 := \left\|\nu\triangle\mathbf{L}_{in} - \sum_{i=1}^d [\mathbf{L}_{in}]_i\partial_{x_i}\mathbf{L}_{in}\right\|_{H^{-1}(\Omega)}^2 + \left\|\nu\triangle\mathbf{L}_{bc} - \sum_{i=1}^d [\mathbf{L}_{bc}]_i\partial_{x_i}\mathbf{L}_{bc}\right\|_{H^{-1}(\Omega)}^2.$$

In addition, provided that

$$|c(\mathbf{w},\mathbf{L}_{in},\mathbf{w})| + |c(\mathbf{w},\mathbf{L}_{bc},\mathbf{w})| \leq \frac{\nu}{2}\|\mathbf{w}\|_1^2 \quad \text{for all } \mathbf{w}\in\mathcal{Y} \quad (4)$$

and

$$\nu^2 > 4\,C_d\,\|\widetilde{f}(\mathbf{L}_{in},\mathbf{L}_{bc})\|_{-1}, \quad (5)$$

where $C_d > 0$ *is the Sobolev embedding constant s.t.* $|c(\mathbf{v},\mathbf{w},\mathbf{z})| \le C_d\|\mathbf{v}\|_1\|\mathbf{w}\|_1\|\mathbf{z}\|_1$ *for all* $\mathbf{v},\mathbf{w},\mathbf{z} \in \mathcal{Y}$*, then the solution* $\mathbf{v}$ *is unique and depends continuously on the boundary data* $(\mathbf{u}_{in}, \mathbf{u}_{bc})$*.*

To pose the optimal design problem, several cost functionals depending on the state solution $(\mathbf{v}, p)$ have been proposed in literature for the optimization of arterial bypass grafts or otherwise regularization of flows where recirculation and vortex generation are to be minimized. By denoting Ω_{obs} the subdomain where physical indices of interest are observed, we list some typical choices together with references to previous works where such functionals have been employed:

1. *viscous energy dissipation* [25, 33]

$$J_1(\mathbf{v}) := \frac{\nu}{2}\int_{\Omega_{\text{obs}}} |\nabla\mathbf{v}|^2\, d\Omega \quad \text{or} \quad J_1(\mathbf{v}) := \frac{\nu}{2}\int_{\Omega_{\text{obs}}} \varepsilon(\mathbf{v}) : \varepsilon(\mathbf{v})\, d\Omega,$$

being $\varepsilon(\mathbf{v}) = (\nabla\mathbf{v} + \nabla\mathbf{v}^T)/2$ the Cauchy strain tensor;

2. *Stokes-tracking type functional* [22, 20, 25]

$$J_2(\mathbf{v}) := \int_{\Omega_{\text{obs}}} |\mathbf{v} - \mathbf{v}_{\text{Stokes}}|^2\, d\Omega,$$

where $\mathbf{v}_{\text{Stokes}}$ is the solution of (1) obtained after neglecting the term $c(\mathbf{v},\mathbf{v},\mathbf{z})$;

3. *vorticity*[2, 4, 22, 25, 38]

$$J_3(\mathbf{v}) := \frac{\nu}{2}\int_{\Omega_{\text{obs}}} |\nabla\times\mathbf{v}|^2\, d\Omega,$$

4. *Galilean invariant* vortex measure for two-dimensional flows [20, 22, 25]

$$J_4(\mathbf{v}) := \int_{\Omega_{\text{obs}}} \max\{\det(\nabla\mathbf{v}), 0\}\, d\Omega \quad \text{or} \quad J_4(\mathbf{v}) := \int_{\Omega_{\text{obs}}} g(\det(\nabla\mathbf{v}))\, d\Omega,$$

where $g(z)$ is a smooth nonnegative function satisfying $g(z) = 0$ for $z \le 0$ and $g(z) = \mathcal{O}(z)$ as $z \to \infty$ [22]. This choice is motivated by the fact that vortex cores are related to regions where the eigenvalues of $\nabla\mathbf{v}$ are complex, and in the two-dimensional case this is equivalent to $\det(\nabla\mathbf{v}) > 0$.

5. *wall shear stress gradient* [27]

$$J_5(\mathbf{v}) := \int_{\Gamma_{\text{obs}}} \nabla\left(\nu\frac{\partial\mathbf{v}}{\partial\mathbf{n}}\cdot\mathbf{t}\right)\cdot\mathbf{t}\, d\Omega, \tag{6}$$

where $\mathbf{n}$ and $\mathbf{t}$ are the unit normal and tangent vectors respectively.

All of the above functionals are bounded in $[H^2(\Omega)]^d$, and the functionals J_1-J_4 are bounded in $[H^1(\Omega)]^d$. The energy functionals J_1 are analytically the simplest to handle. They are coercive and weakly coercive owing to the Poincaré and Korn inequalities respectively[b]. The tracking functional J_2 is suitable only for low-Reynolds flows with negligible convective effects. The vorticity functional J_3 is the most common choice, but it has the problem that strong shear boundary layers can have a disproportionate weight compared to the vortices. The functional J_4 is not differentiable and needs to be regularized to make it regular enough to use the standard optimal control framework. The functional J_5 contains second-order derivatives of velocity evaluated on the boundary, which makes its computation from finite elements approximations difficult. Based on these considerations, we concentrate in the numerical examples on three cost functionals: the viscous energy dissipation J_1, the vorticity J_3, and the vortex measure J_4.

2 A boundary optimal control formulation for bypass design

A first possible approach for the optimal design of bypass grafts is based on the solution of a suitable optimal control (OC) problem in the vein of [4, 6, 15, 20, 24], for which the control function is the Dirichlet boundary condition representing the flow entering into the artery from the graft on the boundary[c] Γ_{bc}. Thus the geometrical properties of the bypass graft are only represented by the velocity profile $\mathbf{u}_{\text{bc}} \in \mathcal{U}_{\text{bc}}$ imposed at the bypass anastomosis, which has to be controlled in order to minimize a given cost functional. This entails the solution of a problem on a *frozen*, fixed domain – the one given by the occluded artery – on which the state Navier-Stokes equations (now representing a constraint), have to be solved. For simplicity we refer also to problems following this formulation as design problems, even if they only involve boundary control.

If the residual flow function $\mathbf{u}_{\text{in}}$ through the occluded section Γ_{in} is known, the *deterministic design (OC) problem* can be formulated as follows: given $\mathbf{u}_{\text{in}}$, find the boundary control function $\mathbf{u}_{\text{bc}}$ solving

$$\min_{\mathbf{u}_{\text{bc}} \in \mathcal{U}_{\text{bc}}} J(\mathbf{v}; \mathbf{u}_{\text{bc}}, \mathbf{u}_{\text{in}}) \quad \text{s.t.} \tag{DD-OC}$$
$$\mathcal{A}(\mathbf{v}, p, \boldsymbol{\eta}; \mathbf{z}, q, \boldsymbol{\lambda}; \mathbf{u}_{\text{bc}}, \mathbf{u}_{\text{in}}) = 0, \quad \forall\, (\mathbf{z}, q, \boldsymbol{\lambda}) \in \mathcal{Y} \times \mathcal{Q} \times \mathcal{G},$$

where $J : \mathcal{Y} \to \mathbb{R}_0^+$ is a cost functional measuring the graft performance (e.g. one of the functionals listed in Sect. 1) and $\mathcal{A}(\cdot; \cdot; \mathbf{u}_{\text{bc}})$ is the Navier-Stokes operator

[b] Coercivity holds at least if $\Omega_{\text{obs}} = \Omega$. If $\Omega_{\text{obs}} \subsetneq \Omega$, as is usually the in practice as we want to focus the reduction to a subregion near the anastomosis, we do not have analytical results but typically the convexity and coercivity of the cost functional is preserved as we shall see in the results section.

[c] With respect to the general case presented in Sect.1, here Γ_{bc} is a (fictitious) boundary representing the anastomosis (see Fig. 2).

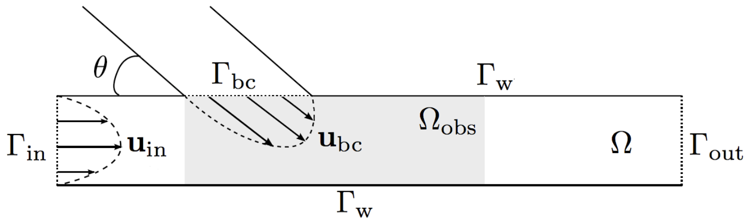

Figure 2: Domain and boundary segments for the optimal boundary control formulation

defined in (2). Here the dependence of the state equation and the cost functional on the control variable $\mathbf{u}_{\mathrm{bc}}$ and the residual flow $\mathbf{u}_{\mathrm{in}}$ has been highlighted.

On the other hand, assuming that the patency of the occluded artery (and the corresponding residual flow $\mathbf{u}_{\mathrm{in}}$) is uncertain, we consider the following worst-case design problem:

> *Find the bypass control function $\mathbf{u}_{bc}$ in such a way that it minimizes the worst-case value of $J(\mathbf{v})$ over all admissible values of the residual flow function $\mathbf{u}_{in}$.*

To obtain a satisfactory answer to this problem, we study the so-called *robust design problem*: find the boundary control function $\mathbf{u}_{\mathrm{bc}}$ solving the worst-case optimization problem

$$\min_{\mathbf{u}_{\mathrm{bc}}\in\mathcal{U}_{\mathrm{bc}}} \max_{u_{\mathrm{in}}\in\mathcal{U}_{\mathrm{in}}} J(\mathbf{v};\mathbf{u}_{\mathrm{bc}},\mathbf{u}_{\mathrm{in}}) \quad \text{s.t.} \tag{RD-OC}$$
$$\mathcal{A}(\mathbf{v},p,\boldsymbol{\eta};\mathbf{z},q,\boldsymbol{\lambda};\mathbf{u}_{\mathrm{bc}},\mathbf{u}_{\mathrm{in}}) = 0, \quad \forall\,(\mathbf{z},q,\lambda)\in\mathcal{Y}\times\mathcal{Q}\times\mathcal{G}.$$

The robust design problem can be understood as a one-shot game, where the designer of the bypass plays first and chooses the control function $\mathbf{u}_{\mathrm{bc}}$ to minimize the cost functional J. The second player then follows by choosing the residual flow function $\mathbf{u}_{\mathrm{in}}$ to maximize the cost function J. The payoff for the designer is $-J$ and for the second player J. Thus the optimal strategy for the designer is given as the solution of a min-max type of strategy obtained by solving (RD-OC), while the second player will choose his response by solving another problem. We call this the *complementary uncertainty problem* and it is defined as: given a known boundary control function $\mathbf{u}_{\mathrm{bc}}$, find the residual flow function $\mathbf{u}_{\mathrm{in}}$ maximizing the cost functional

$$\max_{\mathbf{u}_{\mathrm{in}}\in\mathcal{U}_{\mathrm{in}}} J(\mathbf{v};\mathbf{u}_{\mathrm{bc}},\mathbf{u}_{\mathrm{in}}) \quad \text{s.t.} \tag{CU}$$
$$\mathcal{A}(\mathbf{v},p,\boldsymbol{\eta};\mathbf{z},q,\boldsymbol{\lambda};\mathbf{u}_{\mathrm{bc}},\mathbf{u}_{\mathrm{in}}) = 0, \quad \forall\,(\mathbf{z},q,\lambda)\in\mathcal{Y}\times\mathcal{Q}\times\mathcal{G}.$$

Concerning the well-posedness of these problems, a general existence result for the first optimality problem (DD-OC) can be found in [15] (see Lemma 2.1 and the related proof):

Theorem 1. *Assume that the cost functional* $J(\mathbf{v})$

i) is bounded, i.e. there exists $C_0 > 0$ *s.t.* $J(\mathbf{v}) \leq C_0 \|\mathbf{v}\|_1^2$*;*

ii) is convex, i.e. for any $\mathbf{u}_1, \mathbf{u}_2 \in [H^1(\Omega)]^d$ *and* $\gamma \in [0,1]$ *it holds that* $(1-\gamma)J(\mathbf{u}) + \gamma J(\mathbf{u}) \geq J((1-\gamma)\mathbf{u} + \gamma\mathbf{u})$*;*

iii) satisfies for some constants $C_1, C_2, C_3 > 0$ *the weak coercivity inequality*

$$J(\mathbf{v}) \geq C_1 \|\mathbf{v}\|_1^2 - C_2 \|\mathbf{v}\|_1 - C_3 \quad \textit{for all } \mathbf{v} \in \mathcal{Y}. \tag{7}$$

Let the admissible set $\mathcal{U}_{bc}$ *for the control function be a closed and convex subset of* $[H^{1/2}(\Gamma_{bc})]^d$*. Then the problem* (DD-OC) *admits at least one optimal solution.*

The well posedness of the third problem (CU) is ensured by the following result:

Theorem 2. *Assume that* Γ_{in} *is an open and connected subset of* $\partial\Omega$*, and that the cost functional* $J(\mathbf{v})$

i) is bounded (see (i), Thm. 1) ;

ii) is upper semicontinuous, i.e. $\limsup_{\mathbf{v}\to\mathbf{v}^*} J(\mathbf{v}) \leq J(\mathbf{v}^*)$ *for all* $\mathbf{v}^* \in \mathcal{Y}$*.*

Let the admissible set $\mathcal{U}_{in} \subseteq \mathcal{U}_{C_1}$ *be a closed subset of*

$$\mathcal{U}_{C_4} := \left\{ \mathbf{u} \in [H^2(\Gamma_{in})]^d \ : \ \|\mathbf{u}\|_2 \leq C_4 \right\} \tag{8}$$

for some $C_4 > 0$ *small enough such that (4) is satisfied, and furthermore that the viscosity is large enough to satisfy (5). Then the problem* (CU) *admits at least one optimal solution.*

Proof. Since Γ_{in} is a bounded domain, the embedding $H^2(\Gamma_{\text{in}}) \hookrightarrow H^1(\Gamma_{\text{in}})$ is compact by Rellich's theorem and $\mathcal{U}_{\text{in}}$ is compact in $[H^1(\Gamma_{\text{in}})]^d$. According to Lemma 1, the solution map $\mathbf{u}_{\text{in}} \mapsto \mathbf{v}(\mathbf{u}_{\text{in}})$ is continuous in the H^1-topology under our assumptions. Thus the image of $\mathcal{U}_{C_4}$ given by the Navier-Stokes resolvant operator (2) is a compact set in $\mathcal{Y}$. A bounded upper semicontinuous functional attains its maximum in a compact set. □

It is clear that for coercive cost functionals satisfying (7) the maximizer of (CU) will be found on the boundary of the set of admissible functions $\mathcal{U}_{\text{in}}$. Thus we expect to find maximizers that become increasingly singular as we increase C_1 in (8). In case a near-complete occlusion is not expected, the admissible set of residual flow functions can be regularized to rule out extreme singular cases. In this case we can use the knowledge about the solutions of the (CU) to design a reasonable set of admissible residual flow functions that still contain some level of uncertainty while being mathematically better behaved. We return to this consideration in the numerical examples section.

Existence of solutions for the worst-case problem (RD-OC) in the infinite-dimensional case has not been extensively studied. In a recent paper [19], the authors used the concept of weak lower semi-continuity for set-valued functions to prove existence results for optimal control problems of PDEs for functionals of the min-max type. In the case that the admissible set of residual flow profiles $\mathcal{U}_{\text{in}}$ does not depend on the control variable $\boldsymbol{u}_{\text{bc}}$, and therefore a sufficient condition for the weak lower semi-continuity of

$$\widehat{J}(\boldsymbol{u}_{\text{bc}}) := \sup_{\boldsymbol{u}_{\text{in}} \in \mathcal{U}_{\text{bc}}} J(\boldsymbol{u}_{\text{bc}}, \boldsymbol{u}_{\text{in}})$$

is that $J(\,\cdot\,, \boldsymbol{u}_{\text{in}})$ is weakly lower semi-continuous for all admissible $\boldsymbol{u}_{\text{in}} \in \mathcal{U}_{\text{in}}$ (Theorem 2.5 of [19]). This assumption of independence does not strictly hold in our problem, due to the condition (3) inducing a dependence of $\mathcal{U}_{\text{in}}$ on $\mathbf{u}_{\text{bc}}$, so further study of the well-posedness of the min-max formulation would be needed.

Several approaches can be used for the solution of the optimal control problems discussed throughout this section. Standard techniques are based on iterative optimization schemes based on the gradient of the cost functional, such as the steepest descent method (in this case, at each iteration, the control variable is updated in order to step along the opposite direction of the gradient of the cost functional). This entails the repeated solution, until convergence of the procedure, of the PDEs system obtained as first order necessary optimality conditions *Euler-Lagrange system.* To obtain this system, we can exploit the Lagrangian functional approach [14]: by formally differentiating the Lagrangian and looking for its stationary points, we obtain the simultaneous set of state equations, adjoint state equations, and the equation expressing the optimality condition. Indeed, for the numerical solution of optimal control problems, two different paradigms can be adopted: *(i) optimize-then-discretize*, where we first apply the iterative method, then we discretize the various steps of the algorithm, or *(i) discretize-then-optimize*, where we first discretize our optimal control problem and then we apply an iterative algorithm to solve its discrete version. In any case, the gradient of the cost functional can be replaced by a suitable numerical approximation, and its Hessian by e.g. quasi-Newton approximations if more advanced nonlinear programming techniques can be exploited. Within this strategy – employed to obtain the numerical results presented later on – we just require an efficient tool for evaluating PDE solutions and cost functionals.

3 A robust shape optimization formulation for bypass design

An alternative approach for the optimal design of bypass grafts relies on the solution of a shape optimization (SO) problem, for which the control variable is the shape of the domain Ω itself. This entails the minimization of a cost functional by finding the optimal shape of the domain where the PDE is defined.

In general, this problem features more difficulties than OC problems, such as shape deformation, shape derivatives and the evaluation of shape-dependent quantities; a crucial aspect is the geometrical treatment of the shapes during the optimization process too. In an abstract setting, our problem can be formulated as the following *deterministic design (SO)* problem:

$$\min_{\Omega \in \mathcal{O}_{\rm ad}} J(\mathbf{v}; \Omega, \mathbf{u}_{\rm in}) \quad \text{s.t.} \tag{DD-SO}$$
$$\mathcal{A}(\mathbf{v}, p, \boldsymbol{\eta}; \mathbf{z}, q, \boldsymbol{\lambda}; \Omega, \mathbf{u}_{\rm in}) = 0, \quad \forall\, (\mathbf{z}, q, \boldsymbol{\lambda}) \in \mathcal{Y}(\Omega) \times \mathcal{Q}(\Omega) \times \mathcal{G}(\Omega),$$

where $\mathbf{u}_{\rm in}$ is a given residual flow function, $\mathcal{O}_{ad} \subseteq \mathcal{O}$ denotes a set of admissible shapes among family of all possible shapes $\mathcal{O}$ (to be specified next). The dependence of the state equation and the cost functional on the domain Ω has now been made explicit. As in the optimal control case, a second interesting shape optimization problem is that of a bypass graft design which is *robust* with respect to the residual flow $\mathbf{u}_{\rm in}$ across the occluded branch. In this case, finding the optimal shape of the graft in presence of the worst case scenario in terms of residual flow consists in solving the following *robust design (SO)* problem:

$$\min_{\Omega \in \mathcal{O}_{\rm ad}} \max_{\mathbf{u}_{\rm in} \in \mathcal{U}_{\rm in}} J(\mathbf{v}; \Omega, \mathbf{u}_{\rm in}) \quad \text{s.t.} \tag{RD-SO}$$
$$\mathcal{A}(\mathbf{v}, p, \boldsymbol{\eta}; \mathbf{z}, q, \boldsymbol{\lambda}; \Omega, \mathbf{u}_{\rm in}) = 0, \quad \forall\, (\mathbf{z}, q, \lambda) \in \mathcal{Y}(\Omega) \times \mathcal{Q}(\Omega) \times \mathcal{G}(\Omega), \tag{9}$$

Verifying the well-posedness of shape optimization problems involves additional assumptions of regularity on admissible shapes and continuity of the state solution with respect to shape deformations. Provided that in any domain $\Omega \in \mathcal{O}$ we can solve the state problem uniquely, we can introduce a mapping U that with any $\Omega \in \mathcal{O}$ associates the state solution $U(\Omega) = (\mathbf{v}, p)(\Omega)$, i.e. $U : \Omega \mapsto U(\Omega) \in \mathcal{V}(\Omega)$. Moreover, let $\{\Omega_n\}_{n=1}^{\infty} \subset \mathcal{O}$ be a sequence converging to $\Omega^* \in \mathcal{O}$, $U_n \equiv U(\Omega_n) \in \mathcal{V}(\Omega_n)$; denote as well $\Omega_n \xrightarrow{\mathcal{T}} \Omega^*$ and $U_n \rightsquigarrow U$ two suitable notions of convergence[d] (in the latter case convergence involves different functional spaces, defined on the sequence $\{\Omega_n\}_{n=1}^{\infty}$). Focusing for the sake of simplicity on the shape optimization problem (DD-SO), for a given residual flow $\mathbf{u}_{\rm in}$, the following existence result holds (see for example [18], Theorem 2.10):

Theorem 3. *Let $\mathcal{G} = \{(\Omega, U(\Omega)), \forall\, \Omega \in \mathcal{O}_{ad}\}$ be the graph of the mapping $U(\cdot)$ restricted to $\mathcal{O}_{ad}$. Assume that*

i) $\mathcal{G}$ is compact, i.e. for any sequence $\{(\Omega_n, U(\Omega_n)) \in \mathcal{G}\}_{n=1}^{\infty}$, there exists a subsequence, denoted with $\{(\Omega_{n_k}, U(\Omega_{n_k})) \in \mathcal{G}\}_{k=1}^{\infty}$, and an element $(\Omega^*, U(\Omega^*)) \in \mathcal{G}$, such that $\Omega_{n_k} \xrightarrow{\mathcal{T}} \Omega^*$, $U(\Omega_{n_k}) \rightsquigarrow U(\Omega^*)$ for $k \to \infty$;

ii) the cost functional $J(U; \Omega)$ is lower semicontinuous, i.e. if $\Omega_n \xrightarrow{\mathcal{T}} \Omega^*$ and $U_n \rightsquigarrow U^*$, then $\liminf_{n\to\infty} J(U_n; \Omega_n) \geq J(U^*; \Omega^*)$.

Then problem (DD-SO) *has at least one solution.*

[d] A possible choice for the topology of $\mathcal{O}$ is the set distance topology of Hausdorff.

We point out that the first assumption of the theorem is usually shown by proving (i.a) the compactness of $\mathcal{O}_{\rm ad}$ in the topology τ and (i.b) the continuity of the state solution $U(\Omega)$ with respect to shape variation, i.e. if $\Omega_n \xrightarrow{\tau} \Omega^*$ then $U(\Omega_n) \rightsquigarrow U(\Omega^*)$. Not only, in order to show the continuity of the state solution w.r.t. shape, additional regularity properties have to be introduced on the set of admissible shapes; with this respect, a common assumption is to consider the family $\mathcal{O} \equiv \mathcal{O}_\varepsilon$ of domains with a uniformly Lipschitz boundary (or that equivalently satisfy the so-called uniform ε-cone condition [18]). Additional constraints (e.g. on the volume of the admissible domains) might also be imposed. See e.g. [16] for more details in the Navier-Stokes case. Compactness of the set $\mathcal{O}_{\rm ad}$ can be obtained straightforward if the admissible shapes are obtained from a reference domain through deformations described by perturbations of the identity, i.e. if $\mathcal{O}_{\boldsymbol{\theta}} = \{\Omega = T(\tilde{\Omega}) = (I + \boldsymbol{\theta})(\tilde{\Omega})\}$ being $\boldsymbol{\theta}$ a regular vectorial field whose norm $\|\boldsymbol{\theta}\|_{W^{1,\infty}} < 1$ (see [3], Lemma 6.13); this will be the case of the Free-Form Deformation (FFD) technique, exploited in the numerical tests presented in Sect. 6. The numerical solution of a shape optimization problem can be obtained by the same approach used for optimal control problems. Additional difficulties arise from shape-dependent quantities: for example, the shape derivative of the cost functional, which provides the optimality condition and depends *a priori* on the shape derivatives of state variables, can be written in a more simple way by exploiting the adjoint problem. The shape deformation stage during optimization requires special care, several techniques may be used in this respect.

4 Computational and geometrical reduction strategies

In practice, for both optimal control and shape optimization problems the standard adjoint-based approach will be too computationally expensive. Substantial computational saving becomes possible thanks to a*reduced order model* (ROM) which relies on two reduction steps: *(i)* parametrization of the control variables and *(ii)* substitution of the full-order finite element (FE) solution of (2) with a reduced solution obtained by the reduced basis (RB) method [39]. The approximation of viscous steady nonlinear flows through RB methods was first pioneered in [32] and has been analyzed in [7, 8, 35, 42]; more recent applications can be found e.g. in [29] or in [25], where this approach was applied to a problem of femoral bypass graft shape optimization under uncertainty.

First of all we express the *control* functions (either boundary data $\mathbf{u}_{\rm bc} = \mathbf{u}_{\rm bc}(\boldsymbol{\pi})$ or admissible shapes $\Omega = \Omega(\boldsymbol{\pi})$) as a set of *parametric inputs*, depending on p *control parameters* $\boldsymbol{\pi} \in \mathcal{P} \subset \mathbb{R}^p$. This stage is straightforward in the former case, while in the latter a suitable parametrization of the geometry (as well as a change of variable) is required. Besides, uncertainty elements are treated as parametrized quantities too, depending on q additional parameters $\boldsymbol{\omega} \in \mathcal{Q} \subset \mathbb{R}^q$.

In this way, an equivalent parametrized formulation of the deterministic design problems (DD-OC) or (DD-SO) can be derived as follows:

$$\min_{\boldsymbol{\pi}\in\mathcal{P}} J(V(\boldsymbol{\mu});\boldsymbol{\mu}) \quad \text{s.t.} \quad \mathcal{A}(V(\boldsymbol{\mu}),W;\boldsymbol{\mu})=0, \quad \forall\, W\in\mathcal{V}(\tilde{\Omega}), \tag{10}$$

where $\boldsymbol{\mu}=(\boldsymbol{\pi},\boldsymbol{\omega})\in\mathcal{P}\times\mathcal{Q}$, $V(\boldsymbol{\mu})=(\mathbf{v},p,\boldsymbol{\eta})(\boldsymbol{\mu})$, $\mathcal{V}(\tilde{\Omega})$ is a functional space defined on a reference, parameter independent domain $\tilde{\Omega}$ as $\mathcal{V}(\tilde{\Omega})=\mathcal{Y}(\tilde{\Omega})\times\mathcal{Q}(\tilde{\Omega})\times\mathcal{G}(\tilde{\Omega})$. In an optimal control context, $\Omega\equiv\tilde{\Omega}$, while for a shape optimization problem the parametrized domain $\Omega=\Omega(\boldsymbol{\pi})$ is obtained by applying a parametric mapping $T(\cdot;\boldsymbol{\pi})$ to the reference domain. In our case, this map will be built by exploiting the *free-form deformation* (FFD) technique, in which the deformations of an initial design, rather than the geometry itself, are parametrized [26, 30]. In the same way, the robust design problems (RD-OC) or (RD-SO) can be written as follows:

$$\min_{\boldsymbol{\pi}\in\mathcal{P}}\max_{\boldsymbol{\omega}\in\mathcal{Q}} J(V(\boldsymbol{\mu});\boldsymbol{\mu}) \quad \text{s.t.} \quad \mathcal{A}(V(\boldsymbol{\mu}),W;\boldsymbol{\mu})=0, \quad \forall\, W\in\mathcal{V}(\tilde{\Omega}). \tag{11}$$

Then, we replace the expensive, full-order FE solution $V_h(\boldsymbol{\mu})$ of (2) with the inexpensive RB solution; in the case of deterministic OC/SO problems, following the *discretize than optimize* approach, the standard Galerkin FE approximation of (10) is as follows:

$$\min_{\boldsymbol{\pi}\in\mathcal{P}} J_h(V_h(\boldsymbol{\mu});\boldsymbol{\mu}) \quad \text{s.t.} \quad \mathcal{A}(V_h(\boldsymbol{\mu}),W_h;\boldsymbol{\mu})=0, \quad \forall\, W_h\in\mathcal{V}_h(\tilde{\Omega}), \tag{12}$$

where $\mathcal{N}=\mathcal{N}(h)$ is the dimension of the FE space, depending on the mesh size h. The reduced basis method (see [39, 36] for reviews of the method) provides an efficient way to compute an approximation $V_N(\boldsymbol{\mu})$ of $V_h(\boldsymbol{\mu})$ (and related output) by using a Galerkin projection on a reduced subspace made up of well-chosen FE solutions, corresponding to a specific choice $S_N=\{\boldsymbol{\mu}^1,\ldots,\boldsymbol{\mu}^N\}$ of parameter values. Indicating by $\mathcal{V}_N=\text{span}\{V_h(\boldsymbol{\mu}^n),n=1,\ldots,N\}$ the RB space, the RB formulation of (12) is as follows:

$$\min_{\boldsymbol{\pi}\in\mathcal{P}} J_N(V_N(\boldsymbol{\mu});\boldsymbol{\mu}) \quad \text{s.t.} \quad \mathcal{A}(V_N(\boldsymbol{\mu}),W_N;\boldsymbol{\mu})=0, \quad \forall\, W_N\in\mathcal{V}_N. \tag{13}$$

Thanks to the (considerably) reduced dimension $N\ll\mathcal{N}$ of the space obtained from RB approximation, we can provide *rapid responses* in terms of input/output evaluations. This is ensured by an Offline–Online computational strategy and a rapidly convergent RB space assembling, based on a *greedy algorithm* [39]. More precisely, in an expensive Offline stage we prepare a very small RB "database", while in the Online stage, for each new $\boldsymbol{\mu}\in\mathcal{D}$, we rapidly evaluate both the solution and the output. At the outer level, a suitable iterative optimization procedure is performed, now involving a very reduced version of the original problem. On the other hand, the *reliability* of the RB method is ensured by rigorous a posteriori estimations for the error in the RB approximation w.r.t. truth FE discretization [39].

5 Numerical results: boundary optimal control

In this section we present some numerical results about the optimal design of aorto-coronary bypass grafts based on the solution of the optimal control problems analyzed in Sect. 2.

5.1 Two-dimensional boundary control problems

We consider throughout this section a simplified 2D bypass configuration $\Omega = (0,5) \times (0,1)$, where $\Gamma_{\text{in}} = \{(x,y) : x = 0, y \in (0,1)\}$ and $\Gamma_{\text{bc}} = \{(x,y) : x \in (1,3/2), y = 1\}$, respectively, thus considering the graft-to-host diameter ratio to be fixed at its (near-)optimal value 1.5 as discussed in [23]. In order to exploit the reduced framework discussed in the previous section, we make the simplifying assumption that the control functions are parametrized with respect to the anastomosis angle θ and are given by the following parabolic Poiseuille profiles for simplicity:

$$\boldsymbol{u}_{\text{bc}}(x;\theta,\omega) := \frac{16}{9}\left(\frac{7}{6} - \frac{\omega}{6}\right)\left(x-1\right)\left(\frac{3}{2} - x\right)\begin{bmatrix}(\tan\theta)^{-1} \\ -1\end{bmatrix}, \tag{14}$$

where $\theta \in (\theta_{\min}, \theta_{\max})$ and $0 < \theta_{\min} < \theta_{\max} \leq \pi/2$. In this way, the set of admissible[e] boundary controls is defined by $\mathcal{U}_{\text{bc}} := \{\mathbf{u}_{\text{bc}}(x;\theta,\omega) : \theta \in [\theta_{\min}, \theta_{\max}]\}$, being in our case $\theta_{\min} = 15°$ and $\theta_{\max} = 85°$. On the other hand, $\omega \in (0,4)$ is the variable controlling the flux split between the graft and the host vessels: if $\omega = 0$ we have a completely occlusion, while for $\omega = 4$ we have a 50/50 split of total flux between the graft and the host. The control function $\boldsymbol{u}_{\text{bc}}$ is properly rescaled to satisfy (3).

Thus the control variable in the simplified deterministic design problem is reduced to the angle θ of the bypass graft. Also the radius of the bypass could be taken as an optimization variable, in the case that this is under control of the surgeon performing the operation, but in general more complex geometrical properties such as cuff shapes cannot be incorporated into our model problem. Clearly, we are interested in the minimization of the cost functionals $J_1 - J_4$ in the downfield subregion Ω_{obs} where a vortex may occur, leading to possible occlusions after grafting and plaque formation; here $\Omega_{\text{obs}} = \{(x,y) \in \Omega : (x,y) \in (1,4) \times (0,1)\}$ (see Figs. 1-2). The resulting problem is discretized with 14,260 and 1,827 dofs for velocity and pressure, respectively, using $\mathbb{P}_2/\mathbb{P}_1$ finite elements; the dimension of the computed reduced basis space is $N = 54$, thus yielding the possibility to solve a Navier-Stokes problem in a *real time* way (averaged time over 1,000 evaluations is 0.19 seconds). Parametric optimization problems are solved through a Sequential Quadratic Programming (SQP) technique (see [31]).

[e] Concerning the existence results provided in Sect. 2, it is clear that the admissible set $\mathcal{U}_{\text{bc}}$ given by the control functions (14) is closed in $H^{1/2}(\partial\Omega)$. To see that it is also convex, note that $\varphi(\theta) = 1/\tan\theta$ is a continuous function in $\theta \in [\theta_{\min}, \theta_{\max}]$ and its image is a closed interval, therefore convex.

5.1.1 Deterministic design optimal control problem

As a first approximation we assume that the residual flow profile is parabolic, in particular it is defined as $\boldsymbol{u}_{\text{in}}(y;\omega) := \omega y(1-y)\mathbf{e}_1$. This is a typical choice in numerical simulations of arteries yet its justification or effect on the outcomes seems to be rarely considered. We have solved the (DD-OC) problem for 7 different values of $\omega \in [0,3]$ and for 6 different values of the Reynolds number $Re \in (15, 90)$ considered as a further input parameter in the formulation (1); nevertheless, for the sake of simplicity we report here the results for the maximum value experimented, Re = 90. Within the reduced framework illustrated, the solution of 42 optimal control problems takes about 3 hours of CPU time[f], each of them implying about $10 \div 15$ iterations of the optimization procedure.

The optimal angle θ^* obtained by solving the problem (DD-OC) decreases as the magnitude of the residual flow increases. The specific behavior and values of the four cost functionals varies, however, leading to different ranges for $\theta^* = \theta^*(\omega)$. In particular, the vorticity functional J_3 and the Stokes tracking functional J_2 (see Fig. 3) exhibit a stronger convexity and lead to smaller values of the optimal angles: $\theta^* \in (29°, 43°)$ for J_3 and $\theta^* \in (27°, 30°)$ for J_2, respectively, which are very close to values usually treated as optimal for a graft anastomosis [28, 40]. On the other hand, minimization of functionals J_1 and J_4 yields larger values of the optimal angles, perhaps due to their weaker convexity. In Fig. 4 the flows corresponding to the optimal angles for the functional J_3 and $\omega = 0$, $\omega = 1$ are represented. We point out that in the case of total occlusion the main vortex core in the heel region can never be totally eliminated.

5.1.2 Complementary uncertainty optimal control problem

Since the residual flow profile in the (partially) occluded artery might play an important role in the fluid dynamics of a bypass model, instead of using the parabolic profile $\mathbf{u}_{\text{in}}$ we are interested in finding the profile of the worst residual flow so that the optimized graft is *robust* not just to the magnitude of this flow, but also to its profile. To this aim, we solve a relaxed version of the (CU) problem[g], by considering parametrized control functions $\mathbf{u}_{\text{in}}$ under the form

$$\mathbf{u}_{\text{in}}(y;\boldsymbol{\pi}) = \sum_{i=1}^{6} \pi_i \boldsymbol{\phi}_i(y)\mathbf{e}_1$$

being $\boldsymbol{\phi}_1$ the parabolic profile already introduced, $\boldsymbol{\phi}_2 = \exp(-100(y-0.5)^2)$, $\boldsymbol{\phi}_3 = \exp(-100(y-0.25)^2)$, $\boldsymbol{\phi}_4 = \exp(-100(y-0.75)^2)$ three gaussian profiles centered at the points 0.25, 0.5 and 0.75, and $\boldsymbol{\phi}_5 = y(1-y)(y-0.25)$, $\boldsymbol{\phi}_6 = y(1-y)(y-0.75)$ two cubic profiles, where the control parameters $\{\boldsymbol{\pi}_i\}_{i=1}^{6}$ are such that the flux of $\mathbf{u}_{\text{in}}$ is constant. By solving the relaxed (CU) problem, we find

[f] Computations involving RB approximations have been executed on a personal computer with 2 × 2GHz Dual Core AMD Opteron (tm) processors 2214 HE and 16 GB of RAM.

[g] The full RB adjoint-based method for the solution of (CU) is unavailable at this time.

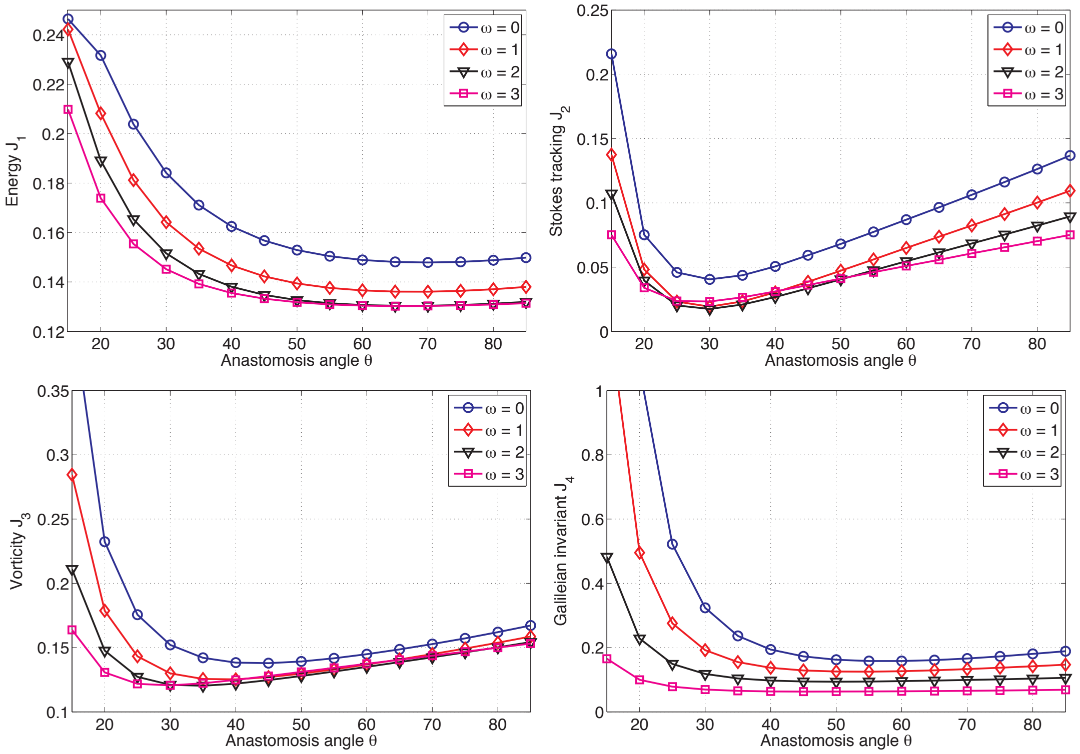

Figure 3: Functionals J_1, J_2, J_3, and J_4 in the subdomain as a function of the anastomosis angle θ for different values of the residual parameter ω with parabolic residual flow.

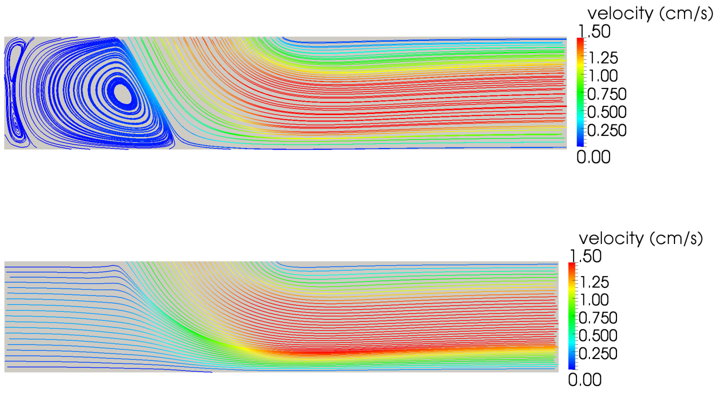

Figure 4: Flow in the optimal configuration for the cost functional J_3, $\omega = 0$ (top) and $\omega = 1$ (bottom), with parabolic residual flow.

that the worst case corresponds to the gaussian profile centered at the midpoint of the occluded section $y = 0.5$, thus corresponding to a severe occlusion in the host artery. The function $\mathbf{u}_{\text{in}} = \omega \exp(-100y^2)\mathbf{e}_1$ will be the boundary condition on Γ_{in} from now on.

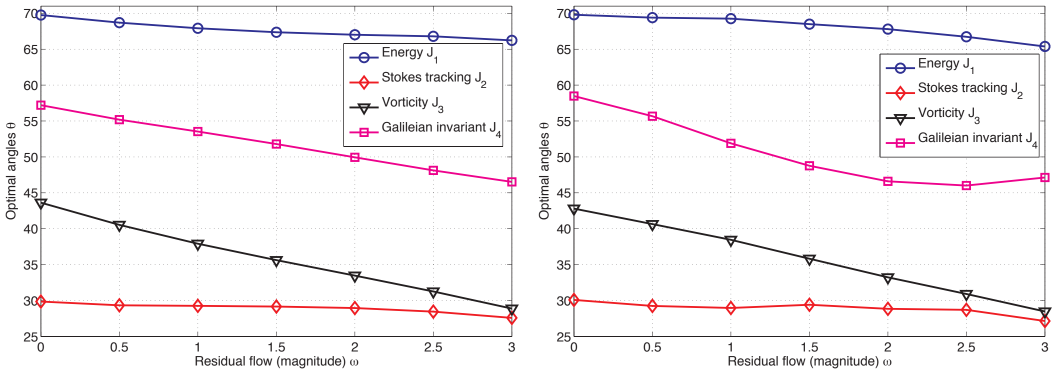

Figure 5: Optimal anastomosis angles as a function of the residual parameter ω for the functionals $J_1 - J_4$, for the parabolic residual flow (left) and the gaussian residual flow (right).

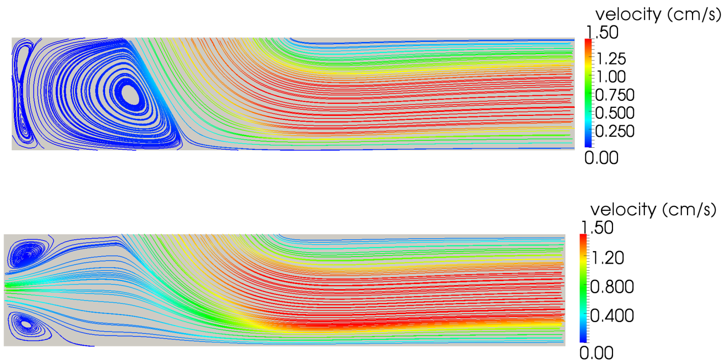

Figure 6: Flow in the optimal configuration for the cost functional J_3, $\omega = 0$ (top) and $\omega = 1$ (bottom), with gaussian residual flow.

5.1.3 Robust design optimal control problem

We can now solve the robust design (RD-OC) problem by considering the same setting as in the (DD-OC) case and the residual flow $\mathbf{u}_{\text{in}}$ given by the gaussian profile obtained by solving the complementary uncertainty (CU) problem. First of all, we consider the deterministic design (DD-OC) problem with a gaussian residual flow: the results, concerning the behavior of the vorticity functional J_3 w.r.t. θ and ω, as well as the optimal angles obtained with the four functionals $J_1 - J_4$, are reported in Fig. 5 for both the parabolic and gaussian residual inflows. The results follow the same trends in both cases, even if flow patterns are remarkably different if the residual flow profile changes. In particular, the gaussian profile induces two secondary vortices near the occlusion, and a more complex vorticity pattern in the anastomosis region.

Two major sources of vorticity can be observed from the streamlines. First, the primary vortex behind the incoming jet, which is generated by the interaction between the fast and slow flows coming into contact at the anastomosis exit. This vortex tends to disappear as we increase θ and/or ω. Secondary vortices are generated by the peak residual flow on both sides of the entry from the occluded branch. However, due to the choice of the observation subdomain, which considers only the flow downstream from the anastomosis, their effect is removed from the vorticity measure: this explains why the results, in terms of optimal angles, are very similar. In Fig. 6 the flows corresponding to the optimal angles for the functional J_3 and $\omega = 0, 1$ are represented.

Finally, the robust design problem (RD-OC) has been solved for the four cost functionals $J_1 - J_4$, providing the results listed in Table 1 (dealing with the most significant J_3 and J_2 cases). Each of these four problems takes approximately $500 \div 700$ seconds to be solved, requiring about $110 \div 150$ input/output evaluations, depending on each case. The robust angles are about the same as the ones obtained as solutions of the deterministic design (DD-OC) problem in the case $\omega = 0$. Hence, the most challenging situation for the minimization of vorticity appears to be the case of total or near-total occlusion of the stenosed branch.

	dimension	profile	$\omega = 0$	$\omega = 1$	$\omega = 2$	$\omega = 3$	robust
J_3	2D	$\mathbf{u}_{\text{in}}$ parabolic	43.6	37.9	33.4	28.9	-
	2D	$\mathbf{u}_{\text{in}}$ gaussian	42.8	38.5	33.2	28.5	42.6
J_2	2D	$\mathbf{u}_{\text{in}}$ parabolic	29.9	29.2	28.9	27.5	-
	2D	$\mathbf{u}_{\text{in}}$ gaussian	30.1	28.9	28.8	27.1	30.0
J_3	3D	$\mathbf{u}_{\text{in}}$ gaussian	45.8	43.8	41.4	38.0	

Table 1: Optimal angles and robust angles θ^* obtained through the (DD-OC) and (RD-OC) problems, vorticity functional J_3 and Stokes tracking functional J_2, both in 2D and 3D.

5.2 Comparison with three-dimensional steady flow

The three-dimensional effects in a steady flow through a bypass anastomosis were considered in [10] and found to be highly significant when it comes to the WSS distribution, especially at higher Reynolds numbers. To test the relevance of 3D effects on the optimal anastomosis angle in our simplified setup, we consider a 3D problem which is assumed plane symmetric along the centerline of the vessel – thus only the half-width of the configuration needs to be meshed. The length and radius of the channel and the bypass are kept the same as in the 2D case, as well as the inflow profiles, which are chosen to be radially symmetric:

$$\begin{aligned} \boldsymbol{u}_{\text{in}}(y, z; \omega) &:= \omega \exp\left[-100\left(y^2 + z^2\right)\right], \\ \boldsymbol{u}_{\text{bc}}(x, z; \theta, \omega) &:= \left(\frac{7}{6} - \frac{\omega}{6}\right)\left[1 - \frac{16}{9}\left(x - \frac{7}{4}\right)^2 + 4z^2\right]\begin{bmatrix}(\tan\theta)^{-1} \\ -1\end{bmatrix}. \end{aligned}$$

We also choose the viscosity in such a way that the Reynolds number is comparable to the highest possible one used in the 2D case, i.e. Re ≈ 80. This is obtained correspondingly to $\nu = 0.0125\, cm^2\, s^{-1}$. The resulting problem is discretized with 196,041 and 65,347 dofs for velocity and pressure, respectively, using $\mathbb{P}_1/\mathbb{P}_1$ finite elements with an interior penalty stabilization scheme [5]. The nonlinear problem (1) is solved starting from the steady Stokes solution and performing pseudo-time stepping until convergence to a steady solution has been achieved. No model reduction was applied in this case and as a result each solution took roughly 20 minutes on 24 parallel 2.66 GHz cores of an Intel Xeon Nehalem cluster.

In Fig. 7(a) we display the obtained value of the vorticity functional J_3 for different values of the parameter ω (other functionals are less meaningful in 3D and are omitted here). optimal angle is located around 45°, but as ω increases the optimal angle θ^* decreases. The qualitative behavior of the vorticity functional J_3 resembles that of the 2D case even if the 3D flow exhibits much more complex flow phenomena, which we will attempt to explain in the following.

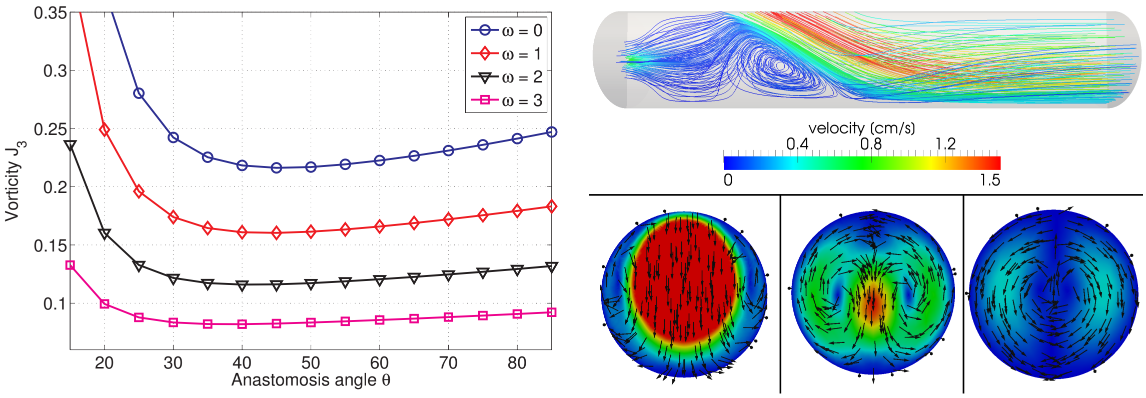

(a) (b)

Figure 7: (a) Vorticity J_3 in the subdomain Ω_{obs} as a function of the anastomosis angle θ for different values of the residual parameter ω in the 3D bypass case. (b) Streamlines of steady flow and transversal velocities at $x = 2.5$, $x = 3.5$, and $x = 4.5$ for the case $\theta = 25°$, $\omega = 1$.

Visualizations of the 3D flow field are reported in Fig. 7(b)–9. Three major sources of vortices can be observed – primary and secondary vortices already remarked for the 2D case, and a tertiary vortex structure. As before, the primary vortex tends to disappear as we increase θ and/or ω (see Fig. 8); of course, in the case of total occlusion, $\omega = 0$, the primary vortex can never be totally eliminated. This fact is demonstrated in Fig. 9, where we display the flow at the maximum angle $\theta = 85°$ but with two different residual flows, $\omega = 0$ (total occlusion) an $\omega = 1$ (strong occlusion). Only in the first case can the primary vortex be observed.

Secondary vortices are generated as in the 2D case by the peak residual flow on both sides of the entry from the occluded branch. Tertiary transversal vortices, the so-called Dean vortices, appear downstream of the anastomosis at moderate Reynolds numbers. While these structures appear exclusively in the 3D flow, it seems their effect on the vorticity functional is an order of magnitude less when compared to the primary vortex, and thus they do not alter the conclusions we obtained earlier based on 2D simulations. The vorticity functional J_3 therefore measures and attempts to control mainly the primary vortex.

In particular, we can remark a strong similarity on the primary and secondary

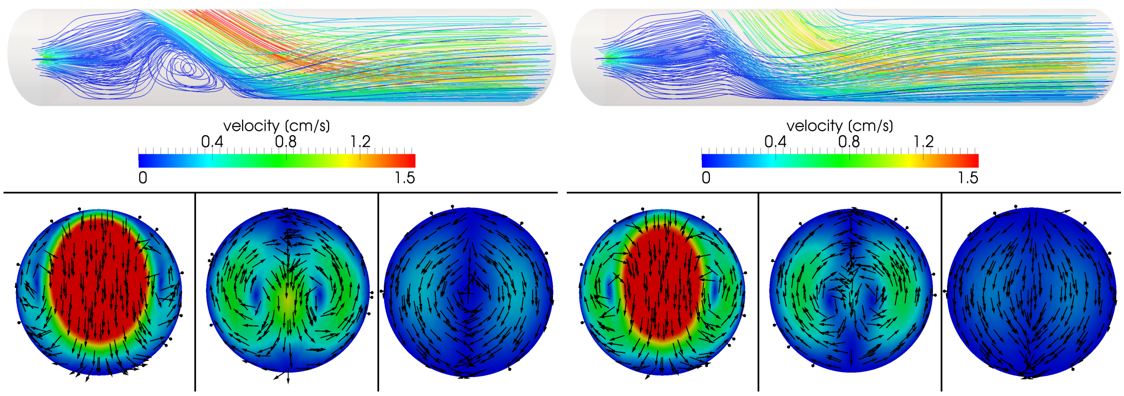

Figure 8: Streamlines of the steady flow and transversal velocities at $x = 2.5$, $x = 3.5$, and $x = 4.5$ for the case $\theta = 30°$ (left) and $\theta = 50°$ (right) with $\omega = 1$. For sufficiently large angles θ the primary vortex disappears, while the secondary and tertiary vortices remain.

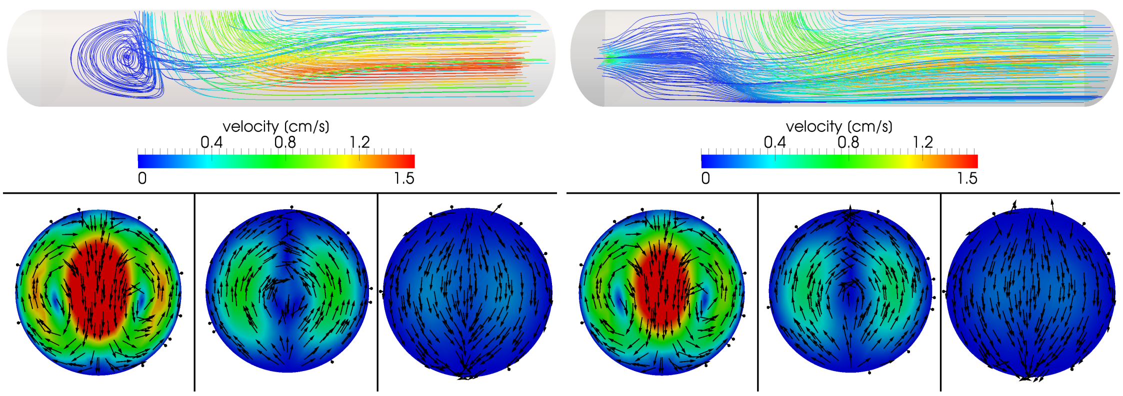

Figure 9: Streamlines of the steady flow and transversal velocities at $x = 2.5$, $x = 3.5$, and $x = 4.5$ for the case $\theta = 85°$ with $\omega = 0$ (left) and $\omega = 1$ (right). In the case of total occlusion, the primary vortex is present even with very large angles.

vortex structures between the 2D and the 3D case, as we can remark in Fig. 10, obtained for the same values of θ and ω already considered in Fig. 7(b)–9. For $\omega \leq 1$ a very strong primary vortex is generated for small angles θ, causing a strongly convex behavior in the functional J_3 as a function of the angle, while for $\omega \geq 3$ the value of the vorticity functional becomes rather insensitive to the choice of the anastomosis angle. Thus we are able to conclude that – similarly to the 2D case – the most challenging situation for the minimization of vorticity is the case of total or near-total occlusion of the stenosed branch. We did not test the effect of the residual flow profile uncertainty on the 3D case as the results in the 2D case already highlighted the need to consider a "worst-case" flow profile in order to obtain robust results. In Table 1 we also include the estimated optimal angles in the 3D case for reference with the 2D results presented before. These were obtained by cubic spline interpolation of the curves in Fig. 7(a). For $\omega = 0$ the optimal angle is very close to the one obtained for the 2D problem, while a divergence of results occurs as ω is increased; the optimal angles in the 3D case tend to be somewhat larger. However, if the robust angle is assumed to correspond in both cases to the optimal angle for $\omega = 0$, we can state that the solution of the robust design problem in 2D gives a good indication to the choice of a robust angle in the more realistic 3D problem.

The remaining question to be answered is, whether the similarity of the 2D and 3D problems in the context of vorticity minimization extends also to the more difficult case of WSS-related functionals, such as J_5 given by (6). It is likely that the tertiary vortices have some effect on the downstream WSS, thus potentially changing the situation between the 2D and 3D cases. While some works on direct minimization of WSS-related quantities have been attempted [9, 40], a rigorous mathematical framework for the minimization of quantities depending on higher derivatives of velocity especially in the uncertainty quantification or robust design context seems beyond the reach of current methodology.

6 Numerical results: shape optimization

Next we present results on the robust design problem using the shape optimization formulation. We consider a parametrized framework based on Free-Form Deformation (FFD), which enables the definition of a set of admissible shapes as diffeomorhpic images of a reference graft shape $\tilde{\Omega}$ through a parametrized map $T(\cdot; \boldsymbol{\pi})$ depending on a set of control points acting as shape design parameters. The reference configuration $\tilde{\Omega}$, represented in Fig. 11, has already been employed for the solution of shape optimization problems with Stokes flows in [30]. In the present case, the FFD parametrization is built on a 5×6 lattice of control points on the rectangle $D = [-1, 3] \times [-0.6, 0.4]$; active control points and their displacements are selected in order to describe a wide family of shapes in terms of the three influential geometrical features already highlighted, i.e. the anastomosis angle, the graft-to-host diameter ratio, and the toe shape.

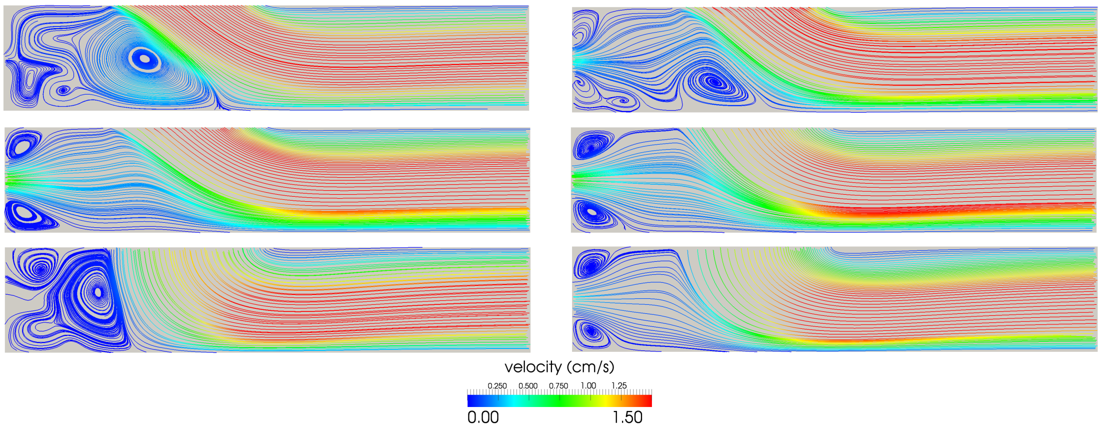

Figure 10: Streamlines of the 2D steady flow for the cases (from top to bottom, from left to right): $\theta = 25°$ with $\omega = 0$, $\omega = 1$; $\theta = 30°$, $\theta = 50°$ with $\omega = 0$; $\theta = 85°$ with $\omega = 0$, $\omega = 1$.

In the end we use a parametrization with $p = 8$ design parameters, which represent the vertical/horizontal displacements of selected control points. These parameters vary in the range $(-\alpha, \alpha)$, $\alpha = 0.15$, for the vertical displacements and in the range $(0, \beta)$, $\beta = 0.6$, for the horizontal displacements of the control points depicted in red/blue in Fig. 11. As before, we consider an observation subregion close to the heel, given here by $\Omega_{\text{obs}} = \{\tilde{\mathbf{x}} = (\tilde{x}_1, \tilde{x}_2) \in \tilde{\Omega} : \tilde{x}_1 \in (1, 2)\}$. In this way, indicating as $\mathcal{P} = \{\boldsymbol{\pi} = (\pi_1, \ldots, \pi_8) \in \mathbb{R}^8 : \ \pi_i \in (-\alpha, \alpha) \ \ \forall i \neq 5, \ \pi_5 \in (0, \beta)\}$ and $V = |D|$, the set of admissible shapes is

$$\mathcal{O}_{\text{ad}} = \left\{ \Omega \subset D \subset \mathbb{R}^2 : \ \Omega = T(\tilde{\Omega}; \boldsymbol{\pi}), \quad \boldsymbol{\pi} \in \mathcal{P}, \ \Gamma_{\text{in}} \cup \Gamma_{\text{bc}} \cup \Gamma_{\text{out}} \text{ is fixed} \right\}.$$

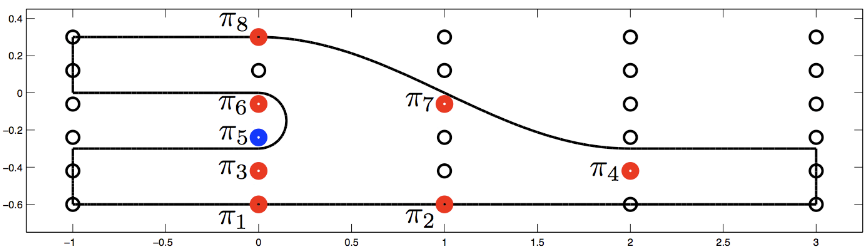

Figure 11: Reference domain Ω and FFD setting. Control points depicted in red/blue can be moved in vertical/horizontal direction.

Concerning inflow profiles, we consider a Poiseuille profile on the inflow Γ_{bc} (graft) and a parametrized gaussian profile $\mathbf{u}_{\text{in}} = \omega\phi(y)\mathbf{e}_1$ on the inflow Γ_{in} (occluded artery), being $\omega \in \mathcal{Q} = [0, \omega_{\max}]$ the uncertainty parameter tuning the degree of occlusion. In particular, the dependence of the two flows on ω is such that the downfield flowrate is constant, with a flow split ranging from 1/0 (complete occlusion of the host artery, for $\omega = 0$) to 2/1 (flowrate across the occluded artery equal to one half of the flowrate across the graft, for $\omega_{\max} = 20$). The resulting problem is discretized with 33,330 and 4,269 dofs for velocity and pressure, respectively, using $\mathbb{P}_2/\mathbb{P}_1$ FE spaces; the corresponding RB approximation is defined on spaces of dimension $N = 36$, thus yielding the possibility to solve a Navier-Stokes problem in a very rapid way (1.84 seconds, averaged time over 1,000 evaluations). As in the OC case, parametric optimization problems are solved through an SQP technique.

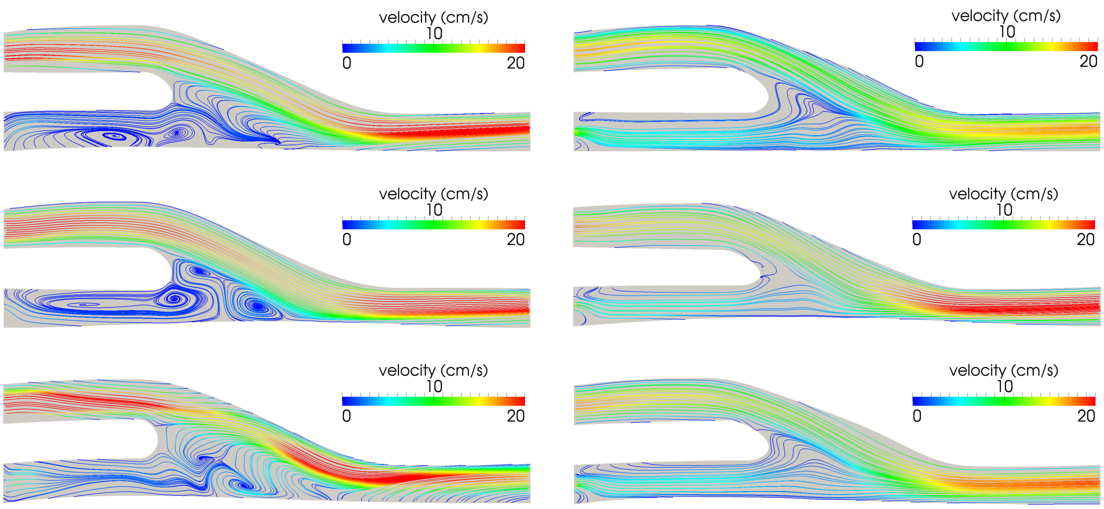

Figure 12: Optimal shapes in the cases $\omega = 0$ (left) and $\omega = \omega_{\max}$ (right) for the vorticity J_3, the Stokes tracking J_2 and the Galileian invariant J_4 functionals (from top to bottom).

In Fig. 12 the velocity fields within the optimal shapes for the vorticity J_3, Stokes tracking J_2 and Galileian invariant J_4 functionals are represented, in the cases $\omega = 0$ (complete occlusion) and $\omega = \omega_{\max}$ (maximum residual flow), respectively. Similarly as in the OC case, the condition leading to the strongest development of vorticity cores is the presence of a complete occlusion, for which the flow through the bypass starts creating a strong and complex vorticity pattern close to the heel. The minimum values of the three cost functionals are decreasing functions with respect to ω, an indication that the case $\omega = 0$ is the most difficult one concerning shape optimization (see Table 2); reduction in the cost functionals ranges from 24% to 70% for the different cases. The vorticity cores are clearly observable also in the optimal configuration in presence of a complete artery blockage; moreover, although we obtain a clear reduction of vorticity also in this case, the vorticity cores never disappear completely. In the end, as for the OC case, we remark that the anastomosis angle decreases as the residual flow increases, since optimal shapes obtained in the case $\omega = \omega_{\max}$ (see Fig. 12) show a more elongated heel.

	$\frac{J^*(\omega=0)}{J^*(\omega=\omega_{\max})}$	ΔJ	# I/O evals	# I/O evals
		$(\omega = 0\,,\, \omega = \omega_{\max})$	$(\omega = 0\,,\, \omega = \omega_{\max})$	(robust)
J_3	1.257	26.3% , 24.2%	125 , 27	389
J_2	1.924	63.2% , 55.3%	99 , 64	416
J_4	1.267	65.4% , 70.7%	183 , 63	973

Table 2: Results for shape optimization (DD-SO) in the cases $\omega = 0$ and $\omega = \omega_{\max}$ and robust shape optimization (RD-SO) problems.

Concerning the solution of the robust design (RD-SO) problem, the robust configurations correspond to the optimal shapes computed for $\omega = 0$ in the previous case. In particular, the solution of the robust (shape) optimization problem requires about $\mathcal{O}(10^3)$ input/output evaluations, thus entailing a CPU time which is at least one order of magnitude larger than a (shape) optimization problem (see Table 2), ranging from $1 \div 4$ hours for the latter case to $13 \div 35$ hours for the former case. This indicates that a design that is robust over the entire range $\omega \in [0, \omega_{\max}]$ must be tuned mainly for the case of total occlusion.

7 Conclusion

We have reviewed the state-of-the art for optimal shape design of arterial bypass grafts. Using mathematical theory of optimal control and shape design, we have proposed two different worst-case optimization formulations to solve the problem of bypass design under uncertainty: (i) a boundary control formulation, which simplifies away the geometry and treats only the angle of the anastomosis as a boundary control variable, and (ii) a shape optimization formulation using a parametrized geometry to represent the anastomosis shape. We applied model reduction in the form of reduced basis methods to reduce the computational costs of solving the robust optimization problems.

We have performed numerical tests to confirm the robustness of the obtained anastomosis angle with respect to the unknown residual incoming flow from the occluded artery. Four different cost functionals taken from literature and proposed for the reduction of downstream vorticity were studied. The optimal anastomosis angle was found to depend strongly on the choice of the cost functional and on the total residual flow from the occluded branch, but not very strongly on the particular shape of the flow profile. We validated our simplified boundary control model by comparing the results obtained against a 3D boundary control problem as well as a 2D shape optimization problem. Three dimensional effects were found not to have a large impact on the total downstream vorticity for moderate Reynolds numbers. The largest vorticity was observed for the case of total occlusion in the host artery. Therefore a robust bypass shape should be one that is tailored for that particular situation.

Acknowledgements

This work was partially funded by the European Research Council Advanced Grant "Mathcard, Mathematical Modelling and Simulation of the Cardiovascular System", Project ERC-2008-AdG 227058. We acknowledge the use of the `rbMIT` package developed by the group of A.T. Patera (MIT) as a basis for the 2D reduced basis simulations. The 3D finite elements simulations presented in this paper have been computed using the open-source `LifeV` library (www.lifev.org). `LifeV` is a joint collaboration between four institutions: École Polytechnique Fédérale de Lausanne (CMCS) in Switzerland, Politecnico di Milano (MOX) in Italy, INRIA (REO, ESTIME) in France, and Emory University (Sc. Comp) in the USA.

References

[1] V. Agoshkov, A. Quarteroni, and G. Rozza. A mathematical approach in the design of arterial bypass using unsteady Stokes equations. *J. Sci. Comput.*, 28(2–3):139–165, 2006.

[2] V. Agoshkov, A. Quarteroni, and G. Rozza. Shape design in aorto-coronaric bypass anastomoses using perturbation theory. *SIAM J. Numer. Anal.*, 44(1):367–384, 2006.

[3] G. Allaire. *Conception optimale de structures*, volume 58. Springer Verlag, 2007.

[4] M. Berggren. Numerical solution of a flow-control problem: Vorticity reduction by dynamic boundary action. *SIAM J. Sci. Comput.*, 19:829, 1998.

[5] E. Burman and M.A. Fernández. Continuous interior penalty finite element method for the time-dependent Navier–Stokes equations: space discretization and convergence. *Numer. Math.*, 107(1):39–77, 2007.

[6] L. Dedè. Optimal flow control for Navier–Stokes equations: drag minimization. *Int. J. Numer. Meth. Fluids*, 55(4):347–366, 2007.

[7] S. Deparis. Reduced basis error bound computation of parameter-dependent Navier-Stokes equations by the natural norm approach. *SIAM J. Num. Anal.*, 46(4):2039–2067, 2008.

[8] S. Deparis and G. Rozza. Reduced basis method for multi-parameter-dependent steady Navier-Stokes equations: Applications to natural convection in a cavity. *J. Comp. Phys.*, 228(12):4359–4378, 2009.

[9] O. Dur, S.T. Coskun, K.O. Coskun, D. Frakes, L.B. Kara, and K. Pekkan. Computer-aided patient-specific coronary artery graft design improvements using CFD coupled shape optimizer. *Cardiovasc. Engr. Tech.*, pages 1–13, 2011.

[10] C.R. Ethier, S. Prakash, D.A. Steinman, R.L. Leask, G.G. Couch, and M. Ojha. Steady flow separation patterns in a 45 degree junction. *J. Fluid Mech.*, 411(1):1–38, 2000.

[11] C.R. Ethier, D.A. Steinman, X. Zhang, S.R. Karpik, and M. Ojha. Flow waveform effects on end-to-side anastomotic flow patterns. *J. Biomech.*, 31(7):609–617, 1998.

[12] D.P. Giddens, H.S. Bassiouny, S. Glagov, and C.K. Zahns. Measurements of velocity and wall shear stress inside a PTFE vascular graft model under steady flow conditions. *J. Biomech. Engr.*, 119:187, 1997.

[13] S. Giordana, S.J. Sherwin, J. Peiró, D.J. Doorly, J.S. Crane, K.E. Lee, N.J.W. Cheshire, and C.G. Caro. Local and global geometric influence on steady flow in distal anastomoses of peripheral bypass grafts. *J. Biomech. Engr.*, 127:1087, 2005.

[14] M.D. Gunzburger. *Perspectives in Flow Control and Optimization*. SIAM, 2003.

[15] M.D. Gunzburger, L. Hou, and T.P. Svobodny. Boundary velocity control of incompressible flow with an application to viscous drag reduction. *SIAM J. Control Optim.*, 30:167, 1992.

[16] M.D. Gunzburger, H. Kim, and S. Manservisi. On a shape control problem for the stationary Navier-Stokes equations. *ESAIM Math. Modelling Numer. Anal.*, 34(6):1233–1258, 2000.

[17] H. Haruguchi and S. Teraoka. Intimal hyperplasia and hemodynamic factors in arterial bypass and arteriovenous grafts: a review. *J. Artif. Organs*, 6(4):227–235, 2003.

[18] J. Haslinger and R.A.E. Mäkinen. *Introduction to shape optimization: theory, approximation, and computation*. SIAM, 2003.

[19] R. Herzog and F. Schmidt. Weak lower semi-continuity of the optimal value function and applications to worst-case robust optimal control problems. *Optim.*, 2011. In press (DOI: 10.1080/02331934.2011.603322).

[20] M. Hintermüller, K. Kunisch, Y. Spasov, and S. Volkwein. Dynamical systems-based optimal control of incompressible fluids. *Int. J. Numer. Meth. Fluids*, 46(4):345–359, 2004.

[21] J.D. Humphrey. Review paper: Continuum biomechanics of soft biological tissues. *Proc. R. Soc. A*, 459(2029):3–46, 2003.

[22] H. Kasumba and K. Kunisch. Shape design optimization for viscous flows in a channel with a bump and an obstacle. In *Proc. 15th Int. Conf. Meth. Models Automation Robotics, Miedzyzdroje, Poland*, pages 284–289, 2010.

[23] R.S. Keynton, M.M. Evancho, R.L. Sims, N.V. Rodway, A. Gobin, and S.E. Rittgers. Intimal hyperplasia and wall shear in arterial bypass graft distal anastomoses: an in vivo model study. *J. Biomech. Engr.*, 123:464, 2001.

[24] K. Kunisch and B. Vexler. Optimal vortex reduction for instationary flows based on translation invariant cost functionals. *SIAM J. Control Optim*, 46(4):1368–1397, 2007.

[25] T. Lassila, A. Manzoni, A. Quarteroni, and G. Rozza. A reduced computational and geometrical framework for inverse problems in haemodynamics. 2011. Technical report MATHICSE 12.2011: `http://mathicse.epfl.ch/files/content/sites/mathicse/files/Mathicse%20reports%202011/12.2011%20TL-GR.pdf`.

[26] T. Lassila and G. Rozza. Parametric free-form shape design with PDE models and reduced basis method. *Comput. Methods Appl. Mech. Engrg.*, 199(23–24):1583–1592, 2010.

[27] M. Lei, J. Archie, and C. Kleinstreuer. Computational design of a bypass graft that minimizes wall shear stress gradients in the region of the distal anastomosis. *J. Vasc. Surg.*, 25(4):637–646, 1997.

[28] F. Loth, P.F. Fischer, and H.S. Bassiouny. Blood flow in end-to-side anastomoses. *Annu. Rev. Fluid Mech.*, 40:367–393, 2008.

[29] A. Manzoni, A. Quarteroni, and G. Rozza. Model reduction techniques for fast blood flow simulation in parametrized geometries. *Int. J. Numer. Methods Biomed. Engng.*, 2011. In press.

[30] A. Manzoni, A. Quarteroni, and G. Rozza. Shape optimization of cardiovascular geometries by reduced basis methods and free-form deformation techniques. *Int. J. Numer. Methods Fluids*, 2011. In press (DOI: 10.1002/fld.2712).

[31] J. Nocedal and S.J. Wright. *Numerical optimization.* Springer Verlag, 1999.

[32] J.S. Peterson. The reduced basis method for incompressible viscous flow calculations. *SIAM J. Sci. Stat. Comput.*, 10:777–786, 1989.

[33] M. Probst, M. Lülfesmann, M. Nicolai, H.M. Bücker, M. Behr, and C.H. Bischof. Sensitivity of optimal shapes of artificial grafts with respect to flow parameters. *Comput. Meth. Appl. Mech. Engrg.*, 199(17-20):997–1005, 2010.

[34] A. Quarteroni and G. Rozza. Optimal control and shape optimization of aorto-coronaric bypass anastomoses. *Math. Models Meth. Appl. Sci.*, 13(12):1801–1823, 2003.

[35] A. Quarteroni and G. Rozza. Numerical solution of parametrized Navier-Stokes equations by reduced basis methods. *Numer. Methods Partial Differential Equations*, 23(4):923–948, 2007.

[36] A. Quarteroni, G. Rozza, and A. Manzoni. Certified reduced basis approximation for parametrized partial differential equations in industrial applications. *J. Math. Ind.*, 1(3), 2011.

[37] A.M. Robertson, A. Sequeira, and M.V. Kameneva. Hemorheology. *Hemodynamical Flows*, pages 63–120, 2008.

[38] G. Rozza. On optimization, control and shape design of an arterial bypass. *Int. J. Numer. Meth. Fluids*, 47(10-11):1411–1419, 2005.

[39] G. Rozza, D.B.P. Huynh, and A.T. Patera. Reduced basis approximation and a posteriori error estimation for affinely parametrized elliptic coercive partial differential equations. *Arch. Comput. Methods Engrg.*, 15:229–275, 2008.

[40] S. Sankaran and A.L. Marsden. The impact of uncertainty on shape optimization of idealized bypass graft models in unsteady flow. *Phys. Fluids*, 22:121902, 2010.

[41] R. Temam. *Navier-Stokes Equations.* AMS Chelsea, Providence, Rhode Island, 2001.

[42] K. Veroy and A.T. Patera. Certified real-time solution of the parametrized steady incompressible Navier-Stokes equations: rigorous reduced-basis a posteriori error bounds. *Int. J. Numer. Meth. Fluids*, 47(8-9):773–788, 2005.

[43] D. Zeng, Z. Ding, M.H. Friedman, and C.R. Ethier. Effects of cardiac motion on right coronary artery hemodynamics. *Ann. Biomed. Eng.*, 31(4):420–429, 2003.

Recent publications :

MATHEMATICS INSTITUTE OF COMPUTATIONAL SCIENCE AND ENGINEERING
Section of Mathematics
Ecole Polytechnique Fédérale
CH-1015 Lausanne

01.2012 A. ABDULLE, A. NONNENMACHER:
A posteriori error estimate in quantities of interest for the finite element heterogeneous multiscale method

02.2012 F. NOBILE, M. POZZOLI, C. VERGARA:
Time accurate partitioned algorithms for the solution of fluid-structure interaction problems in haemodynamics

03.2012 T. LASSILA, A. MANZONI, A. QUARTERONI, G. ROZZA:
Boundary control and shape optimization for the robust design of bypass anastomoses under uncertainty